

Effect of Part Geometry on the Temperature-Dependent Tensile Behavior of LP-DED A6061-RAM2 Aluminum Alloy

Md Faysal Khan^{1,2}, Paul R. Gradl³, Shuai Shao^{1,2}, Nima Shamsaei^{1,2*}

¹National Center for Additive Manufacturing Excellence (NCAME), Auburn University,
Auburn, AL 36849, USA

²Department of Mechanical Engineering, Auburn University, Auburn, AL 36849, USA

³Propulsion Department, NASA Marshall Space Flight Center, Huntsville, AL 35812, USA

* Corresponding author:

Email: shamsaei@auburn.edu

Tel: (334) 844 4839

Abstract

This study investigated the effect of part geometry on the temperature-dependent tensile behavior of A6061-RAM2 aluminum alloy fabricated via laser powder direct energy deposition (LP-DED), using both flat and round specimens. Tensile tests were conducted from cryogenic (-195 °C) to elevated temperatures (up to 400 °C) to evaluate the tensile behavior of each geometry. Under machined surface conditions, round specimens exhibited slightly higher yield strength and comparable ultimate tensile strength, along with a noticeably greater elongation to failure than their flat counterparts. These differences were primarily attributed to geometry-induced constraint effects, as the round specimens minimized corner effects and delayed yielding and necking, which occurred earlier in flat specimens due to reduced material constraint at corners and edges. However, for both geometries, tensile strengths gradually decreased from -195 to 200 °C primarily due to increased dislocation mobility, followed by a sharp strength drop above 200 °C, which was attributed to excessive grain boundary sliding.

Keywords: Laser powder directed energy deposition (LP-DED); A6061-RAM2; Part geometry; Tensile

Introduction

6061 aluminum alloy (A6061) is a widely used precipitation-hardened Al-Si-Mg alloy known for its favorable combination of strength-to-weight ratio, corrosion resistance, and weldability [1,2]. These properties make it highly suitable for critical components in the aerospace, automotive, defense, and marine sectors [3]. In practice, A6061 components are often deployed in environments subjected to a wide temperature range, from cryogenic to elevated, and across a wide range of geometries, from thin-walled sections to larger structural blocks [4,5]. However, in its wrought form, A6061 often suffers from several manufacturing limitations. These include restricted design flexibility, significant material waste during machining, and challenges in fabricating complex geometries or functionally graded structures. Additive manufacturing (AM), with its near-net shaping ability and reduced lead times and costs, has emerged as a potential solution to address these challenges [6,7].

Among different AM techniques, laser powder direct energy deposition (LP-DED) has gained attention for its ability to build large-scale parts and enable repair or hybrid manufacturing [8]. However, A6061 has poor molten state flowability and high solidification shrinkage, which can result in hot tearing and formation of solidification cracks during the LP-DED process [9,10]. These limitations have been mitigated by an approach known as reactive additive manufacturing (RAM), patented by Elementum 3D, which incorporates inoculant particles, such as Ti and B₄C, into the feedstock to refine the microstructure and enhance the solidification behavior [11,12]. For the RAM of A6061, 2 vol.% of such inoculant particles are added to A6061 powder to enable successful deposition via LP-DED.

While a few studies have investigated the mechanical behavior of AM A6061-RAM2 alloy at room temperature [12], limited data exist on how part geometry influences tensile behavior across a wide range of temperatures. The effect of geometry can manifest in two distinct ways. First, during manufacturing, geometric features such as wall thickness and cross-sectional area can significantly impact the thermal history, cooling rate, residual stress development, and defect distribution within the fabricated parts [13,14]. Second, during mechanical testing, specimen geometry influences the measured properties. Therefore, a comparison between parts with flat and round geometries is needed to evaluate the influence of geometry on the temperature-dependent mechanical behavior. This understanding is important for design and qualification of additively manufactured components intended for different service environments.

Therefore, this study investigates the influence of part geometry on the temperature-dependent tensile behavior of LP-DED A6061-RAM2 alloy. Specifically, tensile tests were conducted at -195, 21, 100, 200, 300, and 400 °C, on both flat and round specimens. The failure mechanisms of the alloy for both geometries under tensile loading were also analyzed.

Experimental Procedure

The A6061-RAM2 powder was supplied by Elementum 3D and prepared via vacuum induction gas atomization of pre-alloyed A6061 and subsequent mechanical blending with RAM additives, such Ti and B₄C. The powder particle size range was 53-120 μm , with $D_{10} = 57 \mu\text{m}$, $D_{50} = 80 \mu\text{m}$, and $D_{90} = 119 \mu\text{m}$ (representing the 10th, 50th, and 90th percentile particle sizes, respectively). The chemical composition of the powder, measured via inductively coupled plasma-optical emission spectrometry (ICP-OES), is listed in **Table 1**.

Table 1. Chemical composition of A6061-RAM2 powder (supplied by Elementum 3D) measured via ICP-OES.

Elements	Al	Ti	B	C	Cu	Mg	Si	Fe	Others
wt.%	Bal.	2.10	0.78	0.22	0.26	0.93	0.55	0.06	<0.15

Flat bars measuring 12 mm in width, 3 mm in thickness, and 100 mm in length as well as round bars measuring 12 mm in diameter and 100 mm in length were fabricated vertically via LP-DED using the RPM Innovations (RPMI) 557 laser deposition system. The following process parameters were used for fabrication: laser power of 1500 W, scan speed of 12.7 mm/s, and powder feed rate of 2.7 g/min. Ar was used as a shielding gas during fabrication.

All the bars, both flat and round, underwent multiple heat treatment steps, including hot isostatic pressing (HIP) and T6 treatment (solutionizing and artificial aging). HIP was conducted at 510 °C and an isostatic pressure of 100 MPa for 2 hrs followed by furnace cooling to room temperature. The T6 treatment involved solutionizing at 530 °C for 2 hrs followed by quenching to room temperature and finally aging at 160 °C for 18 hrs followed by air cooling.

Microstructural characterization was conducted on fully heat-treated (HT) coupons excised from the gage section of the flat and round bars on the longitudinal plane. The coupons were mounted using epoxy resin and then ground and polished according to ASTM E3 [15]. The Microscopy was performed at a voltage of 10 kV and a current of 1.5 nA using a Zeiss Crossbeam 550 Scanning Electron Microscope (SEM) equipped with electron backscatter diffraction (EBSD) and energy dispersive X-ray spectroscopy (EDS) detectors. Backscattered secondary electron (BSE) images were obtained using the electron channeling contrast imaging technique.

Both the fully HT flat and round bars were machined into tensile specimens following ASTM E8 (see **Figure 1**). The uniaxial tensile tests were conducted at -195, 21, 100, 200, 300, and 400 °C. The cryogenic, room, and elevated temperature tests were performed according to ASTM E1450, ASTM E8, and ASTM E21, respectively. For cryogenic tests, specimens were immersed in liquid nitrogen until temperature reached to -195 °C and soaked for 5 minutes before pulled to failure. After the failure, the fractured specimens were removed from liquid nitrogen and left in the open air. For elevated temperature tests, a clam-shell radiant heat furnace was used until temperature reached test temperatures and soaked for 30 minutes before pulled to failure. After the failure, the fractured specimens were promptly quenched in water. The tests were performed at a strain rate of 0.005 mm/mm/min. An extensometer was used to measure the axial strain of the specimens until they reached a strain of 0.035 mm/mm. Once this strain was reached, the extensometer was removed due to extensometer travel constraints, and the tests continued under displacement control until the specimens fractured completely. At least three specimens were

tested at room temperature for each heat treatment set, and the average values of tensile properties, i.e., yield strength (YS), ultimate tensile strength (UTS), and elongation to failure (EL), were recorded and reported. After fracture, the surfaces were examined using a SEM to study the fracture mechanisms.

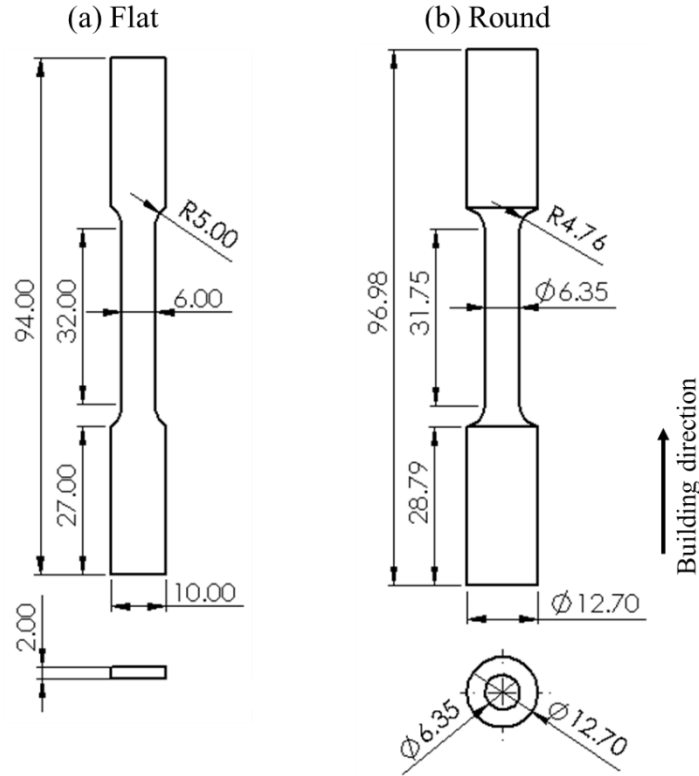


Figure 1. Geometries of LP-DED A6061-RAM2 tensile (a) flat and (b) round specimens following ASTM E8. Note that all the dimensions are in ‘mm’.

Results and Discussion

The microstructure was analyzed for fully HT (HIP+T6) LP-DED A6061-RAM2 coupons (excised from the gage section of both flat and round bars) along the longitudinal plane. As shown in **Figure 2(a)-(b)**, the inverse pole figure (IPF) maps for LP-DED A6061-RAM2 indicate that the grain structure remains nearly identical for both coupons. The grains were equiaxed and fine, with an average grain size of around 6-7 μm . The addition of inoculant particles (e.g., Ti and B_4C) to the A6061 powder promoted heterogenous nucleation during solidification, facilitated by the thermally stable B_4C and the formation of TiC particles. The particles also acted as grain boundary pinners, resisting grain growth and resulting in a fine, equiaxed microstructure. The BSE micrographs in **Figure 2(c)-(d)** show the presence of secondary phase particles, such as TiC and B_4C , which remain unchanged for both coupons. The representative EDS elemental maps for HT coupon from round bar presented in **Figure 3** confirm the presence of TiC and B_4C particles.

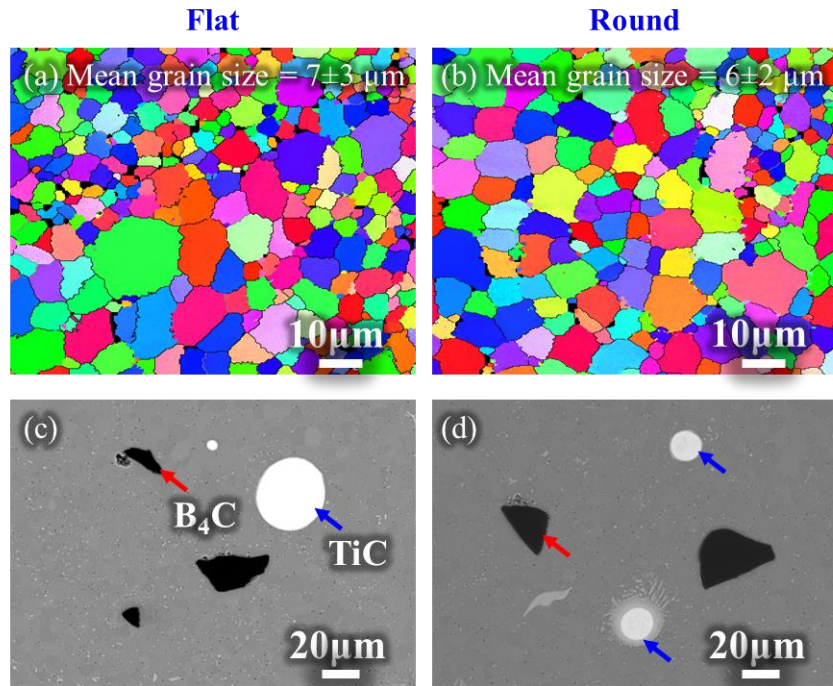


Figure 2. (a)-(b) IPF maps and (c)-(d) BSE micrographs of fully HT LP-DED A6061-RAM2 coupons: (a) and (c) Flat, and (b) and (d) Round.

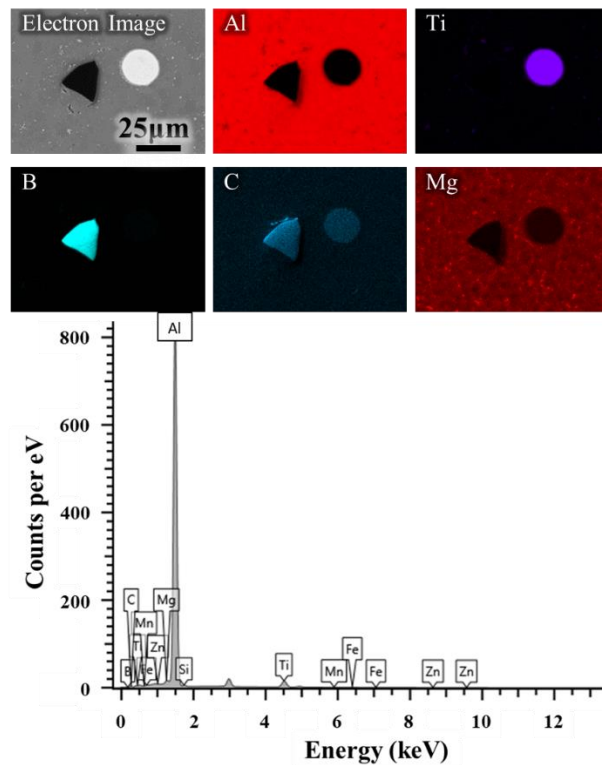


Figure 3. Results from EDS analysis, the elemental maps for LP-DED A6061-RAM2 round bar coupon in fully HT condition.

The representative engineering stress-engineering strain curves of LP-DED A6061-RAM2 flat and round specimens across a temperature range from -195 °C up to 400 °C are plotted in **Figure 4**. In addition, the uniaxial tensile properties, such as YS, UTS, and EL of specimens from both geometries are presented in **Figure 4**. The highest strength was observed at the cryogenic temperature (-195 °C) for specimens from both geometries, which could be attributed to the low dislocation mobility [16]. YS and UTS of both flat and round specimens gradually decreased from -195 to 200 °C and dropped drastically above 200 °C. The gradual reduction in YS up to 200°C could be attributed to a gradual increase in dislocation mobility, and above 200 °C, the drastic drop indicated the activation of another deformation mechanism (e.g., excessive grain boundary (GB) sliding) [16]. YS was higher for round specimens than for flat ones at or below 200 °C and comparable above 200 °C. This strength difference at lower temperatures could be attributed to the corner effects during plastic deformation. While the nominal axial stress under uniaxial loading was uniformly distributed across the cross-section for both geometries, the presence of corners in the flat specimens introduced regions with reduced material constraint to deformation. The intersections of two free surfaces (which are essentially in plane stress) at the specimen corners create conditions favorable for plastic deformation. Additionally, the thinner cross-section of flat specimens (6 mm × 2 mm) may have coupled the corner effects on short sides, further promoting early yielding. At elevated temperatures, however, the role of geometry becomes less significant due to enhanced thermal activation and the dominance of GB sliding deformation mechanisms, leading to comparable YS between both geometries. UTS largely followed a similar trend to YS for both geometries.

Originating from the same corner effects, EL was generally higher for round specimens than for flat ones, suggesting improved ductility under uniaxial loading conditions. Essentially, the conditions in the corners of the flat specimens favoring plastic deformation also created weak regions for material failure. As a result, necking and fracture initiated earlier in flat specimens, leading to lower elongation compared to round specimens. Tensile fractography in **Figure 5** reveals the presence of TiC and B₄C particles on the fracture surfaces for specimens tested from -195 to 200 °C for both geometries. These hard, brittle inoculant particles likely served as preferential void nucleation sites during deformation. However, above 200°C, these particles were no longer visible on the fracture surfaces (see **Figure 5**), which suggested a transition in the dominant fracture mechanism, where GB sliding became increasingly active at elevated temperatures. This thermally activated mechanism promoted more extensive void nucleation, growth, and coalescence along GBs to accommodate the applied deformation and contributed to the measure of higher EL values.

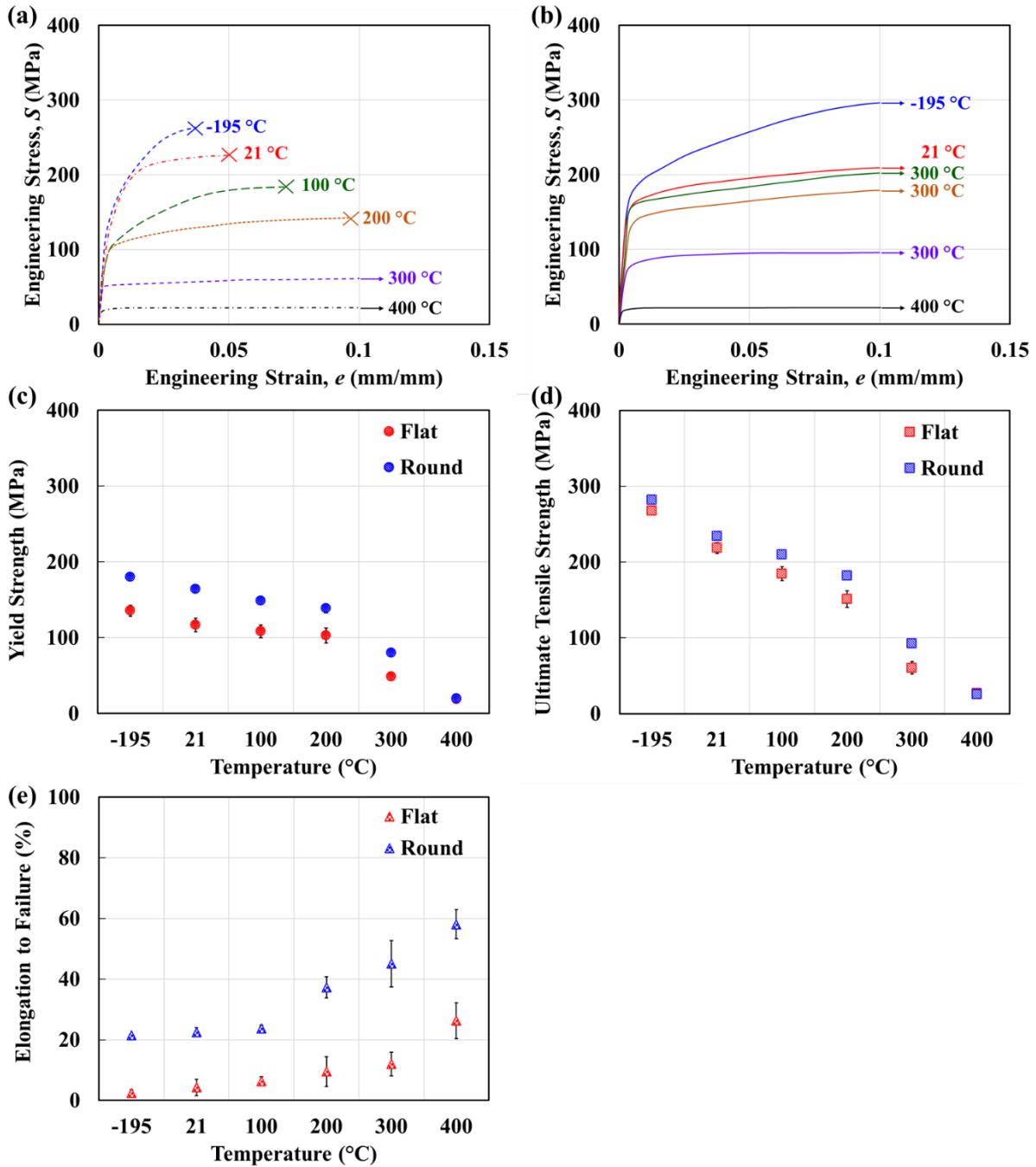


Figure 4. Tensile properties of LP-DED A6061-RAM2 flat and round bars in fully HT condition at different test temperatures of -195, 21, 100, 200, 300, and 400 °C: engineering stress – engineering strain curves for (a) flat and (b) round specimens, (c) YS, (d) UTS, and (e) EL values along with their standard deviation at each temperature.

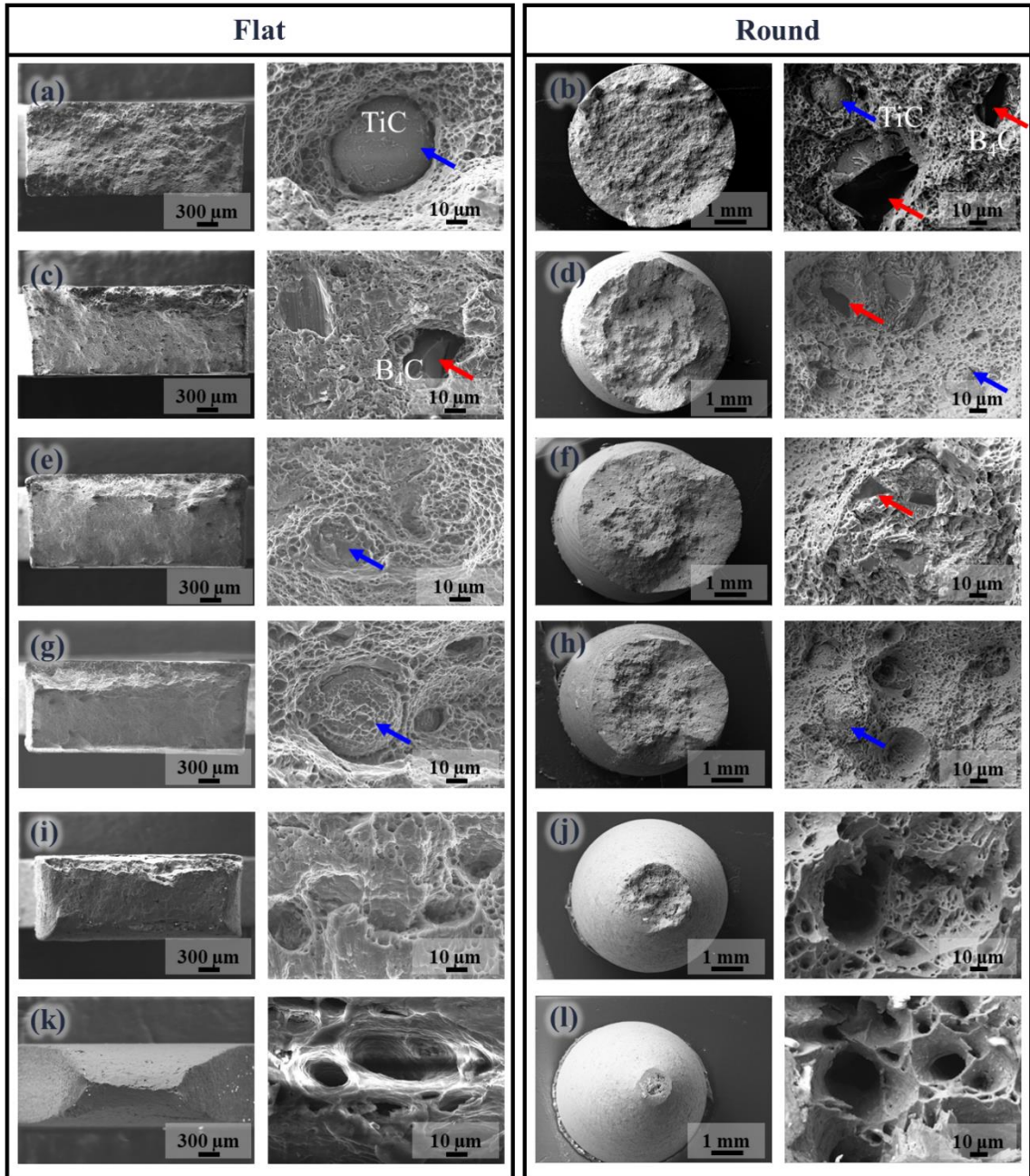


Figure 5. Tensile fracture surfaces of LP-DED A6061-RAM2 (a), (c), (e), (g), (i), (k) flat and (b), (d), (f), (h), (j), (l) round specimens tested at different temperatures: (a)-(b) -195 °C, (c)-(d) 21 °C, (e)-(f) 100 °C, (g)-(h) 200 °C, (i)-(j) 300 °C, and (k)-(l) 400 °C. Blue and red arrows indicate the TiC and B₄C particles, respectively.

Conclusion

This study investigated the part geometry effects on the temperature-dependent tensile behavior of A6061-RAM2 alloy fabricated using laser power direct energy deposition (LP-DED). Tensile tests were conducted for a wide temperature range from -195 to 400 °C on both flat and round specimens. The following conclusions were drawn:

- The inoculant particles, such as Ti and B₄C, aided in grain refinement and formation of fine equiaxed grains during solidification due to the formation of TiC and thermally stable B₄C particles. However, after the heat treatment the particles (i.e., TiC and B₄C) persisted in the microstructure from both geometries, leading to an overall consistent grain structure.
- The yield and ultimate tensile strengths of LP-DED A6061-RAM2 alloy decreased with increasing temperature, with the highest values observed at -195 °C due to limited dislocation mobility. Round specimens showed higher YS than flat ones at or below 200 °C, primarily due to the thinner cross-section of flat specimens coupled with the corner effects promoted early yielding. This geometry-dependent strength difference diminished at higher temperatures as grain boundary sliding became the dominant deformation mechanism.
- Elongation to failure was generally higher for round specimens due to the same corner effects in flat specimens, where the intersections of two free surfaces facilitated plastic deformation and necking, leading to earlier fracture. While EL values were similar between geometries up to 100 °C, ductility increased significantly above 200 °C as grain boundary sliding became the dominant deformation mechanism, replacing void nucleation around brittle inoculant particles (TiC and B₄C) that were prevalent at lower temperatures.

Acknowledgment

This research is based upon the work partially funded by the National Aeronautics and Space Administration (NASA) contract 80MSFC19C0010. Reference herein to any specific commercial product, process, or service by trade name, trademark, manufacturer, or otherwise, does not constitute or imply its endorsement by NASA or the United States Government.

References

- [1] Lee S., Saito Y, Sakai T, Utsunomiya H. Microstructures and mechanical properties of 6061 aluminum alloy processed by accumulative roll-bonding. *Mater Sci Eng A* 2002;325:228–35. [https://doi.org/10.1016/S0921-5093\(01\)01416-2](https://doi.org/10.1016/S0921-5093(01)01416-2).
- [2] Xu B, Yang Z, Meng D, Jia J. Synergistically enhanced strength and plasticity of a 6061 aluminum alloy using hot corrugated constrained groove pressing. *J Alloys Compd* 2025;1014:178682. <https://doi.org/10.1016/j.jallcom.2025.178682>.
- [3] Samuel AU, Araoyinbo AO, Elewa RR, Biodun MB. Effect of Machining of Aluminium Alloys with Emphasis on Aluminium 6061 Alloy – A Review. *IOP Conf Ser Mater Sci Eng* 2021;1107:012157. <https://doi.org/10.1088/1757-899X/1107/1/012157>.

- [4] Grabner F, Österreicher JA, Gruber B, Papenberg N, Gerstner F, Kirnstötter S, et al. Cryogenic Forming of Al-Mg Alloy Sheet for Car Outer Body Applications. *Adv Eng Mater* 2019;21:1900089. <https://doi.org/10.1002/adem.201900089>.
- [5] Summers PT, Chen Y, Rippe CM, Allen B, Mouritz AP, Case SW, et al. Overview of aluminum alloy mechanical properties during and after fires. *Fire Sci Rev* 2015;4:3. <https://doi.org/10.1186/s40038-015-0007-5>.
- [6] Rahman MA, Saleh T, Jahan MP, McGarry C, Chaudhari A, Huang R, et al. Review of Intelligence for Additive and Subtractive Manufacturing: Current Status and Future Prospects. *Micromachines* 2023, Vol 14, Page 508 2023;14:508. <https://doi.org/10.3390/MI14030508>.
- [7] Gradl P, Tinker DC, Park A, Mireles OR, Garcia M, Wilkerson R, et al. Robust Metal Additive Manufacturing Process Selection and Development for Aerospace Components. *J Mater Eng Perform* 2022;31:6013–44. <https://doi.org/10.1007/s11665-022-06850-0>.
- [8] Svetlizky D, Zheng B, Vyatskikh A, Das M, Bose S, Bandyopadhyay A, et al. Laser-based directed energy deposition (DED-LB) of advanced materials. *Mater Sci Eng A* 2022;840:142967. <https://doi.org/10.1016/j.msea.2022.142967>.
- [9] Zhang X, Zheng H, Yu W. A review on solidification cracks in high-strength aluminum alloys via laser powder bed fusion. *Mater Today Proc* 2022;70:465–9. <https://doi.org/10.1016/j.matpr.2022.09.366>.
- [10] Uddin SZ, Murr LE, Terrazas CA, Morton P, Roberson DA, Wicker RB. Processing and characterization of crack-free aluminum 6061 using high-temperature heating in laser powder bed fusion additive manufacturing. *Addit Manuf* 2018;22:405–15. <https://doi.org/10.1016/j.addma.2018.05.047>.
- [11] Nuechterlein JS, Joseph Iten J. Reactive additive manufacturing. US10507638B2, 2021.
- [12] Khan MF, Ghiaasiaan R, Gradl PG, Firdosy S, Shao S, Shamsaei N. Effect of Heat Treatment on the Micro-/Defect-Structure and Tensile Behavior of Additively Manufactured A6061-RAM2 Aluminum Alloy. 2024 Int. SOLID Free. Fabr. Symp., 2024, p. 685–98. <https://doi.org/10.26153/tsw/58106>.
- [13] Yadollahi A, Shamsaei N. Additive manufacturing of fatigue resistant materials: Challenges and opportunities. *Int J Fatigue* 2017;98:14–31. <https://doi.org/10.1016/j.ijfatigue.2017.01.001>.
- [14] Nandi I, Ahmad N, Tilson WG, Wang J, Shamsaei N, Shao S. Crystal plasticity finite element study of tension-induced anisotropic contraction of additively manufactured Haynes 282. *J Mater Sci* 2024;59:4978–94. <https://doi.org/10.1007/s10853-023-09076-0>.
- [15] ASTM E3-11. Guide for Preparation of Metallographic Specimens. *ASTM Stand* 2017;03.01:1–12. <https://doi.org/10.1520/E0003-11R17>.
- [16] Khan MF, Ghiaasiaan R, Gradl PR, Shao S, Shamsaei N. Additively Manufactured Scalmalloy via Laser Powder Bed Fusion (L-PBF): Temperature-Dependent Tensile and Fatigue Behaviors. *Fatigue Fract Eng Mater Struct* 2025;48:1496–513. <https://doi.org/10.1111/ffe.14549>.